Aggregation Properties of Soluble Quinacridones in Two and Three Dimensions

Steven De Feyter,* André Gesquière, and Frans C. De Schryver

Katholieke Universiteit Leuven, Celestijnenlaan 200 F, B-3001 Heverlee, Belgium

Uwe Keller and Klaus Müllen*

Max-Planck-Institut für Polymerforschung, Ackermannweg 10, D-55021 Mainz, Germany

Received February 28, 2001. Revised Manuscript Received September 4, 2001

The aggregation properties of derivatives of linear *trans*-quinacridone, an archetypal pigment, have been explored in two and three dimensions. The sparse solubility of the parent quinacridone pigment in common organic solvents can be traced back to the formation of a network of hydrogen bonds. Introducing aliphatic substituents on specific positions of the quinacridone core leads to an increased solubility without hampering the formation of intermolecular hydrogen bonds. With UV−Vis absorption, steady-state fluorescence, and infrared spectroscopy, the aggregation behavior of these substituted quinacridone derivatives is studied. On the basis of these data, models are proposed for the aggregate structure in solution. In addition, the two-dimensional ordering on graphite of these compounds and *N*,*N*′-dialkylated analogues has been investigated with scanning tunneling microscopy. The comparison between the two-dimensional organization and the solution data allows one to identify the extent of intermolecular interactions involved in the aggregation process.

Introduction

Functional low molecular weight organic materials have gained increasing interest in the past few years because of their possible applications in materials science. Besides acting as mere colorants, they have applications in photovoltaics[1] and in electroluminescent[2] devices. These materials do often not reflect the properties of individual molecules. In contrast, the molecules making part of these optoelectronic materials may form strong intermolecular interactions and the properties of these devices will be governed by the whole collective rather than by individual molecules. To fully exploit the potential of these molecules in organic materials based devices, it is necessary to understand and if possible, to control, the supramolecular packing of a given chromophore.

Linear *trans*-quinacridone[3,4] (**1**, Figure 1) is widely used as an organic pigment. It shows very pronounced photovoltaic[5−7] and photoconductive[8−10] activity and is used as a dopant in electroluminescent devices.[11−25] Despite its attractive electronic properties, only little effort has been put into the development of soluble

* To whom correspondence should be addressed. E-mail: muellen@mpip.mainz-mpg.de; Steven.DeFeyter@chem.kuleuven.ac.be.

(1) Law, K.-Y. *Chem. Rev.* **1993**, *93*, 449.
(2) Kraszovitskii, B. M. *Organic Luminescent Materials*; VCH: Weinheim, 1988.
(3) Lieberman, H. *Liebigs Ann. Chem.* **1935**, *518*, 245.
(4) Labana, S. S.; Labana, L. L. *Chem. Rev.* **1967**, *67*, 1.
(5) Tomida, M.; Kusabayashi, S.; Yokoyama, M. *Chem. Lett.* **1984**, 1305−1308.
(6) Manabe, K.; Kusabayashi, S.; Yokoyama, M. *Chem. Lett.* **1987**, 609−612.
(7) Shichiri, T.; Suezaki, M.; Inoue, T. *Chem. Lett.* **1992**, 1717−1720.
(8) DiMarco, P.; Fattori, V.; Giro, G.; Kalinowski, J. *Mol. Cryst. Liq. Cryst.* **1992**, *216*, 491−497.
(9) Fattori, V.; DiMarco, P.; Giro, G.; Kalinowski, J. *Mol. Cryst. Liq. Cryst.* **1992**, *211*, 313−319.
(10) Hiramoto, M.; Kawase, S.; Yokoyama, M. *Jpn. J. Appl. Phys. Part 2* **1996**, *35*, L349−L351.
(11) Kalinowski, J.; DiMarco, P.; Camaioni, N.; Fattori, V.; Stampor, W.; Duff, J. *Synth. Met.* **1996**, *76*, 77−83.
(12) Tokito, S.; Taga, Y.; Tsutsui, T. *Synth. Met.* **1997**, *91*, 49−52.
(13) Wakimoto, T.; Murayama, R.; Nagayama, K.; Okuda, Y.; Nakada, H. *Appl. Surf. Sci.* **1997**, *114*, 698−704.
(14) Wakimoto, T.; Yonemoto, Y.; Funaki, J.; Tsuchida, M.; Murayama, R.; Nakada, H.; Matsumoto, H.; Yamamura, S.; Nomura, M. *Synth. Met.* **1997**, *91*, 15−19.
(15) Jabbour, G. E.; Kawabe, Y.; Shaheen, S. E.; Wang, J. F.; Morrell, M. M.; Kippelen, B.; Peyghambarian, N. *Appl. Phys. Lett.* **1997**, *71*, 1762−1764.
(16) Tokito, S.; Taga, Y.; Tsutsui, T. *Synth. Met.* **1997**, *91*, 49−52.
(17) Anderson, J. D.; McDonald, E. M.; Lee, P. A.; Anderson, M. L.; Ritchie, E. L.; Hall, H. K.; Hopkins, T.; Mash, E. A.; Wang, J.; Padias, A.; Thayumanavan, S.; Barlow, S.; Marder, S. R.; Jabbour, G. E.; Shaheen, S.; Kippelen, B.; Peyghambarian, N.; Wightman, R. M.; Armstrong, N. R. *J. Am. Chem. Soc.* **1998**, *120*, 9646−9655.
(18) Choi, K. H.; Hwang, D. H.; Lee, H. M.; Do, L. M.; Zyung, T. *Synth. Met.* **1998**, *96*, 123−126.
(19) Sano, T.; Hamada, Y.; Shibata, K. *IEEE J. Sel. Top. Quantum Electron.* **1998**, *4*, 34−39.
(20) Kowalsky, W.; Benstem, T.; Bohler, A.; Dirr, S.; Johannes, H. H.; Metzdorf, D.; Neuner, H.; Schobel, J.; Urbach, P. *Phys. Chem. Chem. Phys.* **1999**, *1*, 1719−1725.
(21) Mattoussi, H.; Murata, H.; Merritt, C. D.; Iizumi, Y.; Kido, J.; Kafafi, Z. H. *J. Appl. Phys.* **1999**, *86*, 2642−2650.
(22) Shaheen, S. E.; Jabbour, G. E.; Kippelen, B.; Peyghambarian, N.; Anderson, J. D.; Marder, S. R.; Armstrong, N. R.; Bellmann, E.; Grubbs, R. H. *Appl. Phys. Lett.* **1999**, *74*, 3212−3214.
(23) Shaheen, S. E.; Kippelen, B.; Peyghambarian, N.; Wang, J. F.; Anderson, J. D.; Mash, E. A.; Lee, P. A.; Armstrong, N. R.; Kawabe, Y. *J. Appl. Phys.* **1999**, *85*, 7939−7945.
(24) Kundu, S.; Fujihara, K.; Okada, T.; Matsumura, M. *Jpn. J. Appl. Phys. Part 1* **2000**, *39*, 5297−5300.
(25) Gross, E. M.; Anderson, J. D.; Slaterbeck, A. F.; Thayumanavan, S.; Barlow, S.; Zhang, Y.; Marder, S. R.; Hall, H. K.; Nabor, M. F.; Wang, J. F.; Mash, E. A.; Armstrong, N. R.; Wightman, R. M. *J. Am. Chem. Soc.* **2000**, *122*, 4972−4979.

10.1021/cm011053y CCC: $22.00
Published on Web 11/30/2001

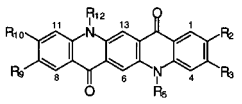

Compound	R_2, R_9	R_3, R_{10}	R_5, R_{12}
1	H	H	H
2	$OC_{12}H_{25}$	$OC_{12}H_{25}$	H
3	$OC_{12}H_{25}$	$OC_{12}H_{25}$	CH_3
4	$OC_{12}H_{25}$	H	H
5	$OC_{12}H_{25}$	H	CH_3
6	OC_6H_{13}	OC_6H_{13}	H
7	$OCH_2CH(C_{11}H_{23})_2$	H	H
8	$OCH_2CH(C_{11}H_{23})_2$	H	CH3

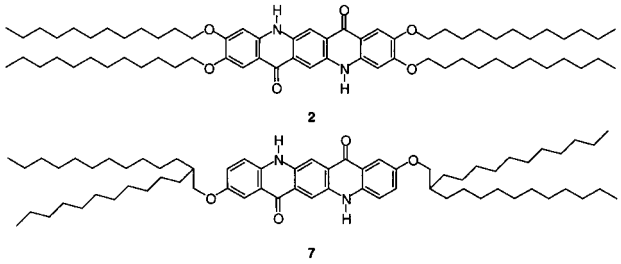

Figure 1. Top: General formula of *trans*-quinacridone. Middle: linear *trans*-quinacridone (**1**) and the derivatives studied (**2**−**8**). Bottom: Chemical structures of **2** and **7**.

derivatives.[23,26−29] The lack of solubility of the pigment can be rationalized by its ability to form infinite networks by hydrogen bond formation. Indeed, **1** is characterized by four hydrogen-bond-forming groups. Its tendency to form aggregates by hydrogen bonding shows up in several polymorphous crystal structures.[30,31] The substitution patterns that lead to an improved solubility so far reported in the literature deal mainly with the introduction of sterically demanding substituents in the 4 and 11 position and/or by *N*-alkylation.[23,26−28] This eliminates the possibility of hydrogen bond formation and, hence, these compounds are highly soluble in common organic solvents but they do not show any tendency toward aggregate formation.

Recently, we reported an approach for synthesizing soluble linear *trans*-quinacridone, 2,3,9,10-tetra(dodecyloxy)quinacridone (**2**, Figure 1), which retains the potential of forming hydrogen bonds.[29] This tendency to form aggregates was expressed by the concentration-dependent spectroscopic properties. When brought into contact with solvents such as THF, $CHCl_3$, and CCl_4 or toluene, **2** swells notably to result in clear, partly gel-like solutions. The color of these solutions varies from yellow to red violet, depending on the chosen concentration of **2**, temperature, and solvent polarity. 2,9-Di-(dodecyloxy)quinacridone (**4**, Figure 1), which carries only two substituents, is only very sparsely soluble (boiling THF) while 2,3,9,10-tetra(hexyloxy)quinacridone (**6**, Figure 1), which possesses the same number of CH_x groups and has the same substitution pattern of **2**, is much more soluble. This observation suggests that the ordering of the molecules in the solid phase differs significantly for both types of compounds. For those QNC derivatives with substituents in the 2, 3, 9, and 10 position, hydrogen bonding might not be optimal because of steric hindrance. In the remainder of the text, QNC stands for the chromophore of the molecule.

To investigate this hypothesis, another 2,9-disubstituted quinacridone derivative, 2,9-di-(2-undecyltridecyl-1-oxy)quinacridone (**7**, Figure 1), has been synthesized and its properties were investigated. This particular substitution pattern was chosen to minimize the steric hindrance and it introduces the same number of CH_x groups as in compound **2**. The aggregation properties in a solution of **7** have been studied by spectroscopic means and have been compared to those of **2**. Structural models for the molecular ordering in aggregated form are suggested upon comparison with spectroscopic and structural properties of crystal polymorphs of **1**.

In addition, the aggregation properties in solution of these substituted quinacridones, including *N*,*N*′-dimethyl-substituted analogues, have been compared with their two-dimensional (2D) ordering on an atomically flat surface as observed by scanning tunneling microscopy (STM). STM has the potential of imaging monolayers at the liquid/solid interface with submolecular resolution.[32−36] These investigations are aimed at gaining more insight into the aggregation structure and the intermolecular interactions leading to aggregation. Comparing the two-dimensional structure as observed with STM and the three-dimensional ordering has proven to be very useful in understanding the intermolecular interactions involved in self-assembly processes.[36−39]

Experimental Section

A. Synthesis. There are three well-established routes, a, b, and c, which lead to *trans*-quinacridones. Methods a and b utilize 1,4-dihydroxy-1,4-cyclohexadiene-2,5-dicarboxylic dialkyl esters, which are subjected to a nucleophilic displacement reaction with 2 equiv of aniline. Route a then proceeds via dehydrogenation of the central cyclohexadiene ring and Friedel−Crafts cyclization of the resulting dianilinoterephthalic acid dialkyl ester. Route b starts in an analogous fashion, the sequence of dehydrogenation and cyclization is, however, reversed, so that 6,13-dihydroquinacridones constitute key intermediates. The synthesis of 2,3,9,10-tetraalkoxy-substituted quinacridones requires 3,4-dialkoxyanilines as intermediates, and it is obvious that the cyclization in either route can afford regioisomers. Route c comprises the reaction of anthranilic acid (2 equiv) with benzoquinone and, again, Lewis-acid-induced cyclization of the resulting 2,5-bis(anthraniloyl)-1,4-benzoquinone. Unlike in routes a and b, intro-

(26) Kitahara, K.; Yanagimoto, H.; Nakajima, N.; Nishi, H. *J. Heterocycl. Chem.* **1992**, *29*, 167−169.
(27) Nakahara, H.; Kitahara, K.; Nishi, H.; Fukuda, K. *Chem. Lett.* **1992**, 711−714.
(28) Nakahara, H.; Fukuda, K.; Ikeda, M.; Kitahara, K.; Nishi, H. *Thin Solid Films* **1992**, *210*, 555−558.
(29) Keller, U.; Müllen, K.; De Feyter, S.; De Schryver, F. C. *Adv. Mater.* **1996**, *8*, 490.
(30) Potts, G. D.; Jones, W.; Bullock, J. F.; Andrews, S. J.; Maginn, S. J. *J. Chem. Soc., Chem. Commun.* **1994**, 2565−2566.
(31) Lincke, G. *Dyes Pigments* **2000**, *44*, 101−122.
(32) Rabe, J.; Buchholz, S. *Science* **1991**, *253*, 424−427.
(33) Frommer, J. *Angew. Chem., Int. Ed. Engl.* **1992**, *31*, 1298−1328.
(34) Cyr, D. M.; Venkataraman, B.; Flynn, G. W. *Chem. Mater.* **1996**, *8*, 1600−1615.
(35) Giancarlo, L. C.; Flynn, G. W. *Annu. Rev. Phys. Chem.* **1998**, *49*, 297−336.
(36) De Feyter, S.; Gesquiere, A.; Abdel-Mottaleb, M. M.; Grim, P. C. M.; De Schryver, F. C.; Meiners, C.; Sieffert, M.; Valiyaveettil, S.; Mullen, K. *Acc. Chem. Res.* **2000**, *33*, 520−531.
(37) EichhorstGerner, K.; Stabel, A.; Moessner, G.; Declerq, D.; Valiyaveettil, S.; Enkelmann, V.; Mullen, K.; Rabe, J. P. *Angew. Chem., Int. Ed. Engl.* **1996**, *35*, 1492−1495.
(38) Valiyaveettil, S.; Mullen, K. *New J. Chem.* **1998**, *22*, 89−95.
(39) Azumi, R.; Gotz, G.; Debaerdemaeker, T.; Bauerle, P. *Chem. Eur. J.* **2000**, *6*, 735−744.

duction of a 3,4-dialkoxyanthranilic acid would then avoid the formation of regioisomers and exclusively produce the desired ("linear") 2,3,9,10-tetraalkoxyquinacridones. This reaction, however, proved unsuccessful so that we had to revert to routes a and b. It is obvious that the analogous synthesis of 2,9-dialkoxyquinacridones requires 4-alkoxyanilines as starting compounds.

The synthesis of 2,3,9,10-tetra(dodecyloxy)quinacridone (**2**) and 5,12-dimethyl-2,3,9,10-tetra(dodecyloxy)quinacridone (**3**) has been reported by us elsewhere.[29]

2,9-Di(dodecyloxy)quinacridone (4). 2,5-Bis-(4-dodecyloxyanilino)terephthalic acid (4.9 g) was subjected to cyclization with trimethylsilyl polyphosphate as previously described by us.[29] 2,9-Di(dodecyloxyquinacridone (**4**) was obtained in quantitative yield as a surprisingly insoluble dark blue solid.

FT-IR (KBR) ν (cm^{-1}): X = 3262, 3251, 3228, 3188, 3166, 3140, 3112, 3096 (NH), 2955−2850, 1690, 1574, 1347, 1257. UV/Vis (DMSO/THF) λ_{max} (log ϵ): 528 (3.94). LD-TOF m/z: 681 (M^+, 100%), 653 (35%; $M^+ - M_{(co)}$). Elemental analysis found % (calcd %): (681.0), C (77.37/77.61), H 9.10 (8.88), N 3.82 (4.11).

5,12-Dimethyl-2,9-di(dodecyloxy)quinacridone (5). Quinacridone (**4**) (300 mg, 0.3 mmol) in a two-phase system consisting of 30 mL of toluene and 10 mL of aqueous NaOH (40%) and 100 mg of tetrabutylammonium hydrogensulfate (0.3 mmol) were heated to reflux with vigorous stirring, whereupon the starting compound dissolved in the organic phase with the formation of the blue dianion. After the solution cooled to about 80 °C, 56 mg of *p*-toluenesulfonic acid methylester (3.0 mmol) was added and the temperature was again increased to reflux with stirring. After 24 h at reflux, the toluene phase was separated while still warm, diluted with 100 mL of chloroform and extracted three times with saturated potassium carbonate solution. After drying and evaporation of the solvent, repeated extraction with hot ethanol gave pure 5,12-dimethyl-2,3,9,10-tetradodecyloxyquinacridone (**5**) in nearly quantitative yield.

mp 101 °C. ^{1}H NMR (200 MHz, C_2, Cl_4, D_4, 120 °C): δ 8.55 (s, 2H, Ar), 7.88 (s, 2H, Ar), 6.63 (s, 2H, Ar), 4.15 (t, ^3J = 6.4 Hz, 4H, $-OCH_2-$), 4.08 (t, J = 6.4 Hz, 4 H, $-OCH_2-$), 3.88 (s, 6H, $-NCH_3$), 2.0−0.8 (m, 92 H, $-CH_2-$, $-CH_3$). ^{13}C NMR (125 MHz, $CDCl_3$, δ): 176.20, 155.90, 145.06, 139.65, 136.00, 125.13, 114.99, 112.82, 108.81, 97.50, 69.48, 69.26, 33.99, 31.90, 29.69−29.11, 26.11, 26.05, 22.64, 14.02. FT-IR (solution in CCl_4) ν (cm^{-1}): 2955−2854, 1604, 1504, 1463, 1296, 1261, 1244. FD-MS m/z: 1076.2.

2,9-Di-(2-undecyltridecyl-1-oxy)quinacridone (7). 2,5-Di-[4(2-undecyltridecyl-1-oxy)anilino]terephthalic acid (1.52 g, 1.35 mmol) was dissolved in 30 mL of anhydrous $CHCl_3$ and heated to reflux with 5 g of trimethylsilyl polyphosphate. Chloroform was then removed under vacuum and the residue heated in an oil bath at 160 °C for 1 h, whereupon the color changed to dark blue. To remove trimethylsilyl polyphosphate, the mixture was poured into 200 mL of aqueous NaOH (10%), heated with stirring and the solid removed by filtration. The aqueous phase was then extracted with chloroform followed by drying with potassium carbonate. Removal of K_2CO_3 and evaporation of the solvent afforded a violet solid that was dissolved in tetrahydrofuran and carefully precipitated by the addition of ethanol. Yield: 1.15 g (84%).

mp < 220 °C. ^{1}H NMR (500 MHz, THF-d_8, 60 °C, δ): 10.33 (s, 2H, NH), 8.42 (s, 2H, ArH), 7.79 (d, ^4J = 3 Hz, 2H, ArH), 733 (d, ^3J = 9 Hz, 2H, ArH), 7.29 (dd, ^3J = 9 Hz, ^4J = 3 Hz, 2H, ArH), 4.00 (d, ^3J = 5.6 Hz, 4H, OCH_2-), 1.85−0.85 (m, 94 H, $-CH_2-$ and $-CH_3$). (125 MHz, $C_2D_2Cl_4$/DMSO-d_6 5:1, 130 °C, δ): 176.57, 152.97, 136.44, 134.02, 124.44, 123.83, 119.21, 117.72, 112.93, 106.67, 71.59, 37.33, 30.74, 28.87−28.07, 25.87, 21.39, 12.78. FT-IR (solution in CCl_4, $c = 2.35 \times 10^{-3}$ mol/L) ν (cm^{-1}): 3263, 3227, 3183, 2926, 2855, 1607, 1568, 1343. FD-MS m/z: 1017.3. Elemental analysis $C_{68}H_{108}N_2O_4$ (1017.6): C 79.87 (80.26), H 11.05 (10.70), N 2.98 (2.75).

5,12-Dimethyl-2,9-di(2-undecyltridecyl-1-oxy)quinacridone (8). The synthesis proceeded as described for compound **5**.

mp 128 °C. ^{1}H NMR (200 MHz, $C_2D_2Cl_4$, 120 °C, δ): 8.58 (s, 2H, Ar), 7.83 (s, 2H, Ar), 4.0 (m, 10H, $-CH_2$, $-NCH_3$) 2.0−0.8 (m, 84H, $-CH-$; $-CH_2-$ and $-CH_3$). ^{13}C NMR (125 MHz, J-modulated spin−echo experiment, negative intensities: (−); C_2D_2Cl, 20 °C, δ): 178.86, 155.55, 139.56, 137.69, 126.98 (−), 123.37, 117.54 (−), 114.49 (−), 109.98 (−), 101.02, 73.69, 39.54 (−), 35.18 (−), 33.16, 33.01, 31.89−30.55, 28.25, 23.47, 15.26 (−). FT-IR (KBr): ν (cm^{-1}) 2956−2851, 1605, 1504, 1463, 1270, 1243. FD-MS m/z: 1045.5.

B. Scanning Tunneling Microscopy. Prior to imaging, all compounds under investigation were dissolved in 1-octanol, 1-phenyloctane, 1,2,4-trichlorobenzene, or a mixture of these (for details, see section B) and a drop of this solution was applied on a freshly cleaved surface of highly oriented pyrolytic graphite. The STM images were acquired in the variable current mode (constant height) under ambient conditions with the tip immersed in the liquid. In the acquired STM images, white corresponds to the highest and black to the lowest measured tunneling current. STM experiments were performed using a Discoverer scanning tunneling microscope (Topometrix Inc., Santa Barbara, CA: now ThermoMicroscopes) along with an external pulse/function generator (Model HP 8111 A), with negative sample bias. Tips were electrochemically etched from Pt/Ir wire (80%/20%, diameter 0.2 mm) in a 2 N KOH/6 N NaCN solution in water.

The experiments were repeated in several sessions using different tips to check for reproducibility and to avoid artifacts. Different settings for the tunneling current and the bias voltage were used, ranging from 0.3 to 1.0 nA and from −10 mV to −1.5 V, respectively. After registration of a STM image of a monolayer structure, the underlying graphite surface was recorded at the same position by decreasing the bias voltage, serving as an in situ calibration. All STM images contain raw data and are not subjected to any manipulation or image processing.

Results and Discussion

A. Aggregation in Solution. A.1. Steady-State Absorption and Fluorescence Spectra. Figure 2 shows the concentration-dependent (A, C) and temperature-dependent (B, D) absorption spectra of **2** in THF and **7** in toluene, respectively. The concentration-dependent absorption spectra are divided by the QNC concentration and therefore reflect the concentration-dependent extinction coefficients. For **2** in THF, the characteristic spectrum of the single quinacridone molecule with its long wavelength maximum at λ = 496 nm is found at concentrations below 1×10^{-4} M (Figure 2A). More concentrated solutions exhibit an additional, red-shifted absorption band at λ = 558 nm, which completely dominates the visible part of the spectrum for concentrations near 1×10^{-3} M. A further increase of the concentration above 3×10^{-3} M does not change the shape of the spectrum, while at intermediate concentrations the relative intensities of the absorption bands change over the entire wavelength region. When dissolved in less polar solvents such as toluene (not shown), **2** exhibits spectroscopic features that correspond to those of the more concentrated THF solutions and the molecules remain aggregated at concentrations below 1×10^{-6} M at room temperature. Compound **7**, on the other hand, does not display aggregation in THF (not shown) up to a concentration of 1 mM. In toluene, however, **7** shows distinct aggregation behavior (Figure 2C). At low concentrations, the absorption spectrum is typical for monomer absorption, with a maximum in the visible region at 526 nm. Increasing the concentration leads to changes similar to those found for **2**. Spectral changes occur throughout the complete absorption

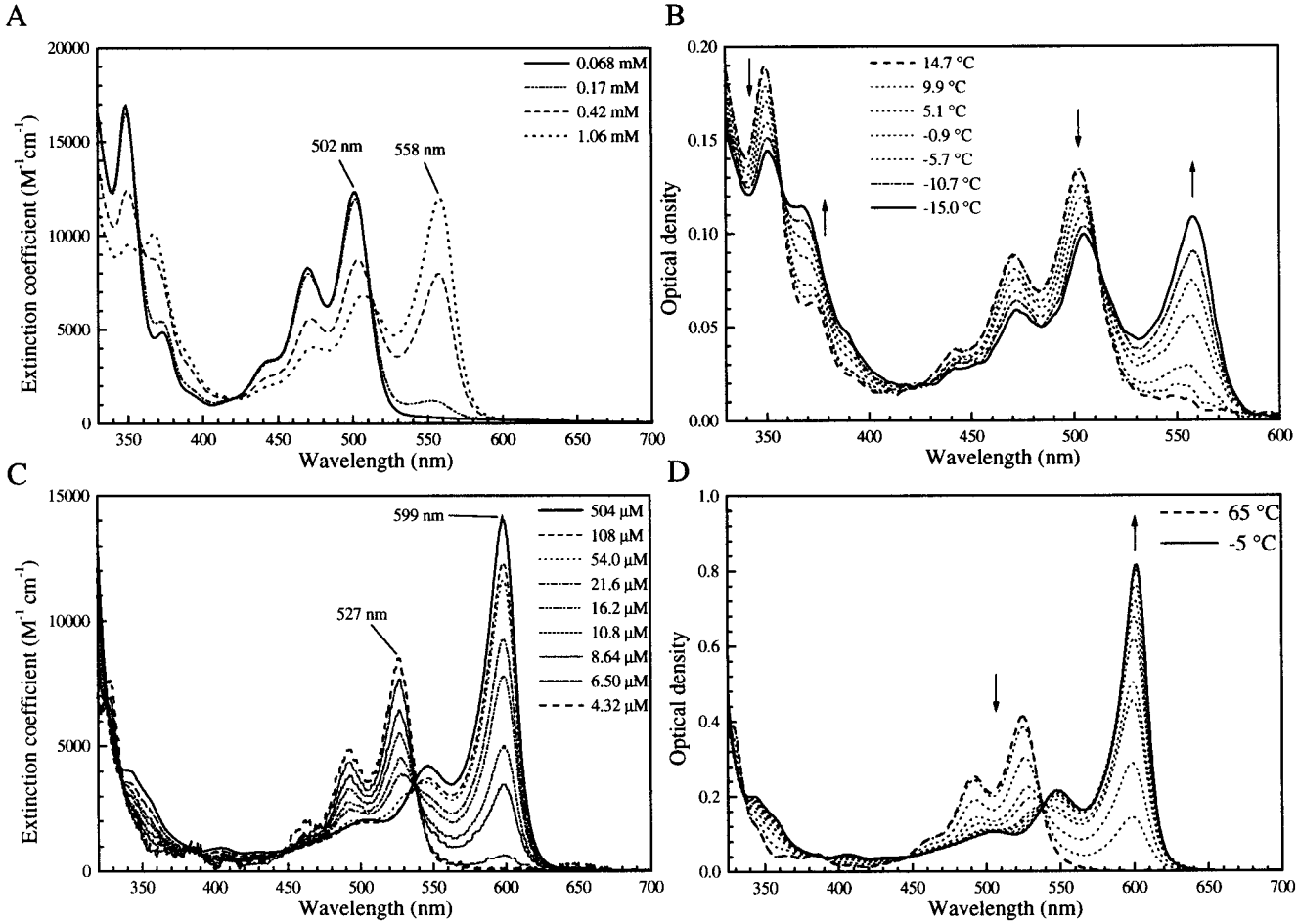

Figure 2. Concentration-dependent (A, C) and temperature-dependent (B, D) absorption spectra of **2** in THF and **7** in toluene, respectively. The absorption spectra are corrected for the compound concentration and reflect the concentration-dependent extinction coefficients.

spectrum and the most striking change is the appearance of a new absorption band at 598 nm. The difference in the position of the maxima of **2** and **7** can be attributed to a difference in substitution pattern. As the absorption spectrum does not considerably change after reaching a certain concentration, one can consider the spectrum at the highest concentration to represent the absorption spectrum of the "aggregate".

Changing the temperature also has an influence on the spectroscopic properties. The spectroscopic changes resulting from decreasing the temperature are similar to those caused by increasing the concentration (Figure 2B,D). Aggregate formation is in both solvents reversible and the temperature dependence shows that aggregation is exothermic: aggregation is favored at low temperature. The spectroscopic properties do not change considerably in the gel-like phase, which is reached at even higher concentrations. This indicates that (i) no aggregates are formed which are characterized by a well-defined aggregation number and (ii) that the spectrosocopic properties of the aggregate are only weakly influenced by the aggregate size. Both in toluene and in THF, **2** shows a higher aggregation tendency than **7**. Several effects could come into play: (i) the solubilizing properties of branched chains are known to be better than those of the linear ones and (ii) the tendency to form hydrogen bonds may differ for both compounds. It is worth noting that the aggregates formed by compound **7** form microcrystals that are characterized by an additional long-wavelength absorption band (632 nm in toluene).

These quincacridone monomers are highly fluorescent ($\Phi_F \sim 0.5$), but upon aggregation, the fluorescence quantum yield drops significantly. The fluorescence quantum yield of **2** in aggregated form equals only 0.002. The monomer and aggregation absorption and fluorescence spectra for **2** and **7** are shown in Figure 3A,B, respectively.

The existence of a multiple equilibrium in solution is revealed from the concentration-dependent fluorescence intensity at the monomer maximum. Figure 4A represents the monomer fluorescence intensity of **2** in toluene at 50 °C as a function of the total concentration and the intensity reflects the free monomer concentration because of the negligible fluorescence quantum yield of the aggregates. At low concentrations, the free monomer fluorescence increases almost linearly with total concentration. The fluorescence intensity levels off at 4×10^{-6} M and reaches a plateau. The concentration-dependent absorption spectra (not shown) under these conditions reveal also the progressive change of a pure monomer solution to a solution containing mainly aggregates. Under these experimental conditions (negligible reabsorption), fluorescence intensity measurements provide an elegant way to determine the free monomer concentration. Figure 4B represents the cal-

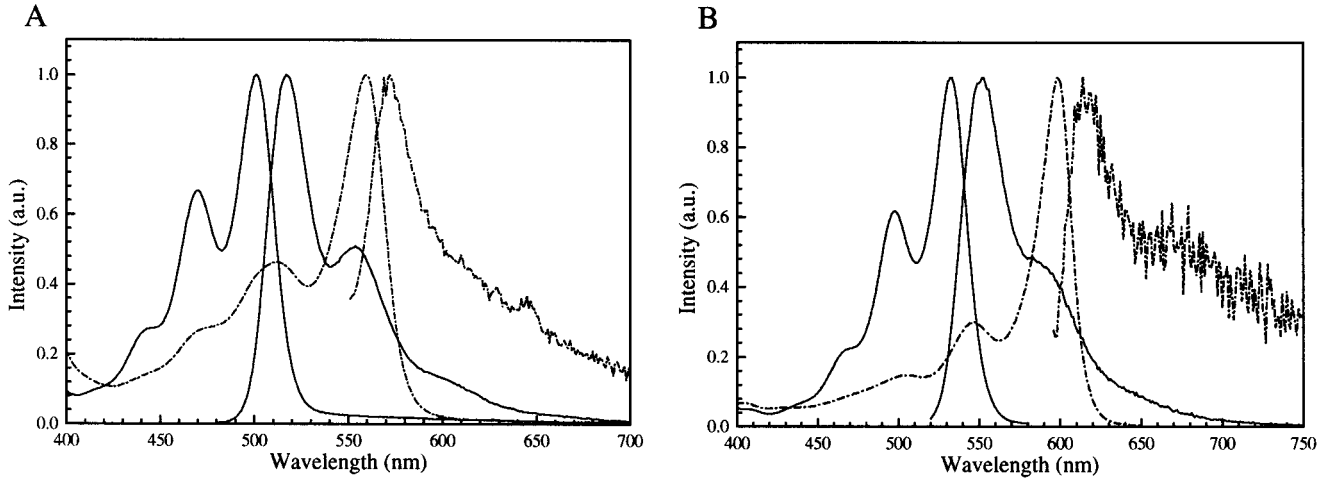

Figure 3. Monomer (solid) and aggregation (dash dot) absorption and fluorescence spectra of (A) **2** and (B) **7**, respectively.

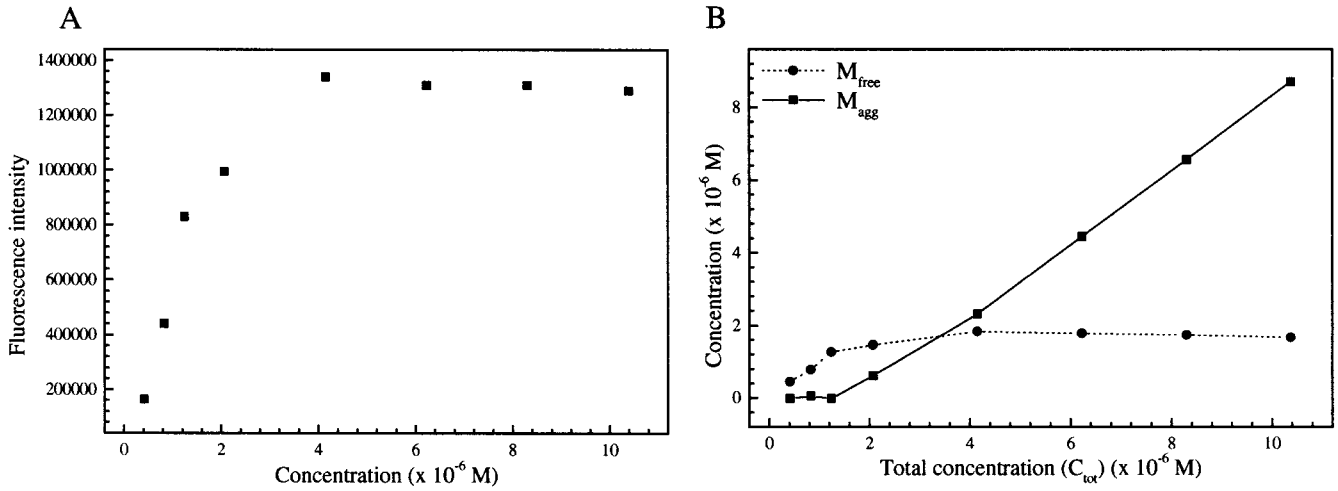

Figure 4. (A) Monomer fluorescence intensity at 509 nm of **2** in toluene at 50 °C as a function of the total concentration of **2**. (B) Calculated concentrations of free monomer (M_{free}) and aggregated monomer (M_{agg}) as a function of the total concentration of **2** based upon (A).

culated concentrations of free monomer (M_{free}) and aggregated monomer (M_{agg}) as a function of the total concentration. For a "one equilibrium" system, the free concentration is expected to increase continuously, instead of reaching a constant value, while the content of an aggregated monomer increases almost linearly with the total concentration. Note that *N*,*N*′-dimethylquinacridone derivatives, such as **3** and **8**, do not show any tendency to aggregation, which indicates that hydrogen bonding is crucial for aggregate formation. Also, the preferential aggregate formation in apolar solvents supports the hypothesis of hydrogen bond formation.

A.2. IR Spectroscopy. The quincacridone pigment (**1**) is known to form different polymorphous structures (alpha, beta, and gamma).[30,31,40,41] These polymorphs differ only slightly in their IR spectra.[42] The IR spectra of the two main crystal modifications, beta-**1** and gamma-**1**, are shown in Figure 5A.[43] These spectra are very similar except for the region between 3000 and 3300 cm^{-1} (Figure 5B), which shows very pronounced differences. This region corresponds to the N−H stretching and this IR band is characterized by six submaxima, which for both crystal modifications can be found at the same position. However, the overall shape of this band is rather symmetric for gamma-**1** but asymmetric for the beta modification. Similarly, the IR spectra of solutions of **2** and **7** containing mainly aggregates have been obtained and have been compared to those of the crystal modifications. The solvent of choice is CCl_4 because of its excellent spectral characteristics for IR spectroscopy (no absorption in the N−H region) and because of its apolar character, which promotes aggregation of the quinacridone derivatives. The IR spectra of **2** (1.5×10^{-3} M) and **7** (2.35×10^{-3} M) are shown in Figure 6A,B, respectively. Their spectra differ considerably in the N−H stretching region. However, they show resemblance to those of the beta- and gamma-**1** polymorphs. The corresponding N−H stretching region of **2** and gamma-**1** and of **7** and beta-**1** are shown as inserts in the respective figures. Although there is no complete correspondence in the fingerprint region, there

(40) Koyama, H.; Scheel, H. J.; Laves, F. *Naturwissenschaften* **1966**, *53*, 700.
(41) Lincke, G. *Farbe Lack* **1980**, *86*, 966.
(42) Filho, D. S.; Oliveira, C. M. F. *J. Mater. Sci.* **1992**, *27*, 5101−5107.

(43) In the case of QNC, at least seven polymorphic forms have been reported on the basis of powder X-ray data, although only three, alpha, beta, and gamma, are widely accepted.[30]

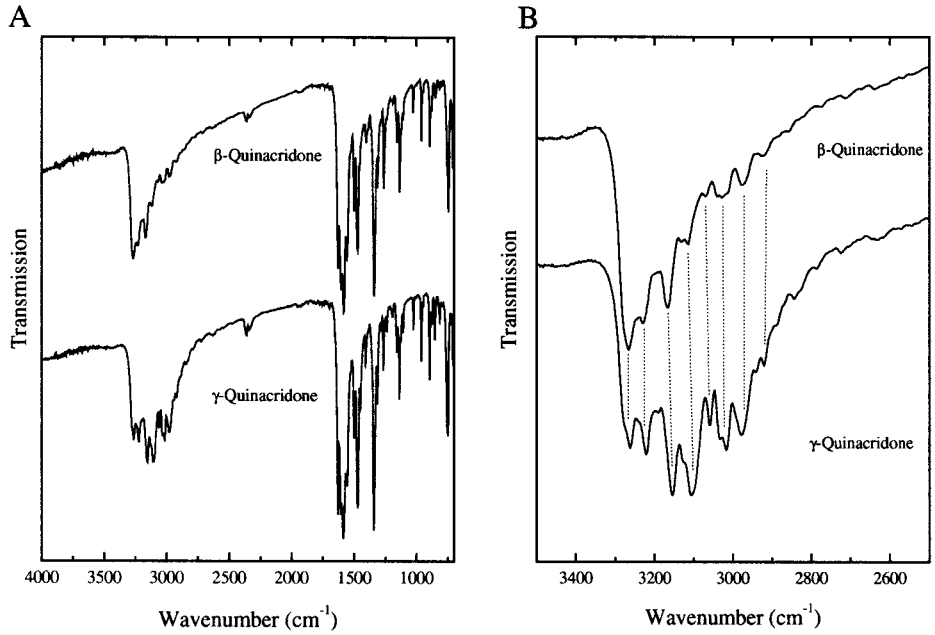

Figure 5. IR spectra of the two main crystal modifications of **1**. (A) beta-**1** and (B) gamma-**1**.

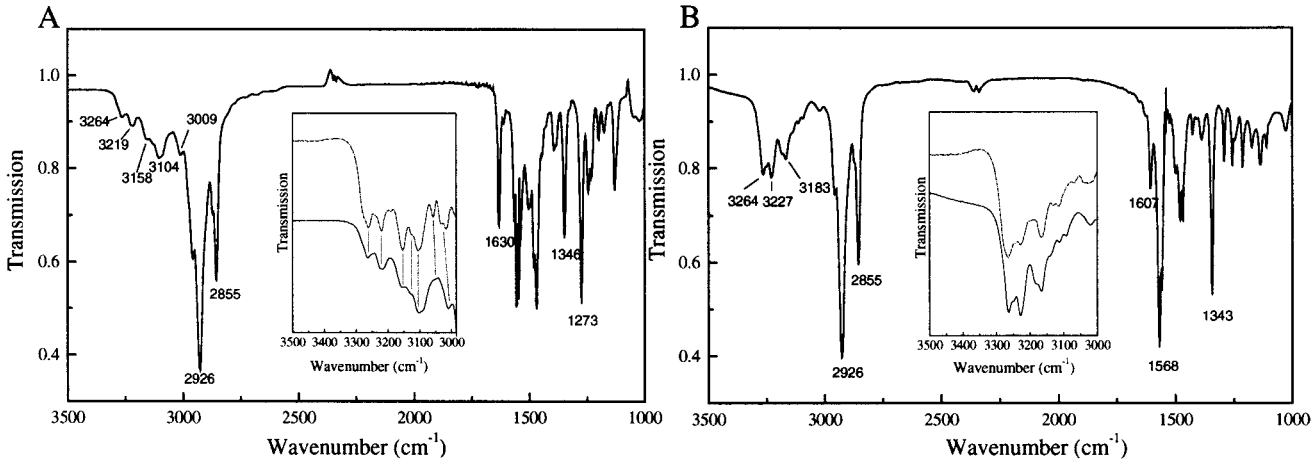

Figure 6. IR spectra of (A) **2** (1.5×10^{-3} M) and (B) **7** (2.35×10^{-3} M) in CCl_4. The corresponding N−H stretch region of **2** (solid) and gamma-**1** (dash dot) and **7** (solid) and beta-**1** (dash dot) are shown as inserts in the respective figures.

is almost perfect agreement between the band shape and the position of the submaxima of the aggregates with those of the respective crystal modifications they are compared with. Note that the appearance of the aggregate spectrum in the N−H region is partly disturbed by the remaining absorption of the C−H stretch. The IR spectrum of a highly diluted solution of **2** in THF-d_8 (not shown) is at one point very different from the aggregate spectrum in CCl_4: the structured absorption spectrum is replaced by a simple band at 3300 cm^{-1}. This is also the case for 1,4,8,11-tetrahexylquinacridon ($R_2 = R_9 = R_3 = R_{10} = R_5 = R_{12} = H$, $R_1 = R_4 = R_8 = R_{11} = C_6H_{13}$), which is not able to form hydrogen bonds. These observations are probably related to differences in molecular packing and in hydrogen bonding. Beta-**1** forms lamellae with the molecules lying in the same plane. These molecules are connected via both H bonds protruding from the sides: every chromophore forms hydrogen bonds with two neighbors (Figure 7A). For gamma-**1**, on the other hand, the hydrogen-bond-forming chromophores are not lying in the same plane; along the hydrogen-bonding direction, the orientation of the chromophores is alternating: every chromophore forms hydrogen bonds with four neighbors (Figure 7B).[30] The high degree of correspondence between the IR spectra of **2** and gamma-**1** and **7** and beta-**1** suggests that the molecular ordering and the hydrogen-bonding pattern in the aggregates resembles those in the respective crystal modifications.

This results in the following proposals for the aggregate structure of compound **2** as depicted in Figure 8A,B. The QNC chromophores form hydrogen bonds with four different adjacent chromophores. This could give rise to a two-dimensional structure (Figure 8A) or a more tubular kind of aggregate (Figure 8B). The hydrogen-bonding pattern within the two-dimensional aggregate is similar to that proposed in Figure 7B. The hydrogen-bonding pattern in the tubular aggregate is somehow different: pairs of (parallel) molecules are stacked on top of each other and each pair is rotated with respect to adjacent pairs.

According to the comparison of the IR spectra of beta-**1** and **7**, the proposed model involves a linear coplanar ordering of the chromophores in the aggregate

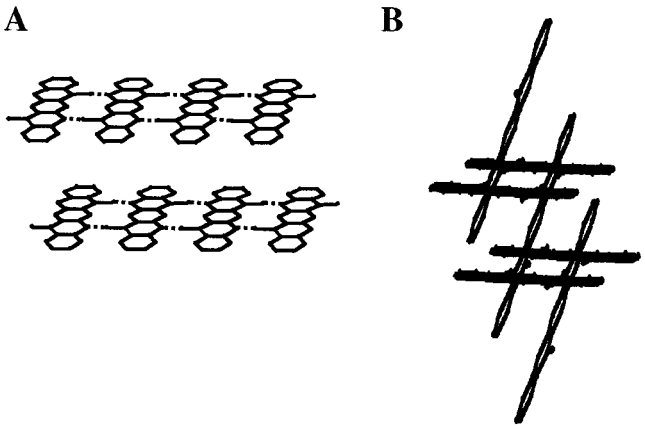

Figure 7. Intermolecular interactions of **1** in 3D. (A) beta-**1**. The molecules "connected" by hydrogen bonds are lying in the same plane. Every molecule forms hydrogen bonds with two neighbors. (B) gamma-**1**. Along the direction of the hydrogen bonds, the orientation of the chromophores is alternating. They are not lying in the same plane. Every molecule forms hydrogen bonds with four neighbors.

(Figure 8C). Such an infinite chain is not supposed to be very stable and it is likely that based upon $\pi-\pi$ interactions, several of these chains can lie on top of each other.

The formation of aggregates at lower concentrations by **2** is in agreement with our proposed model of a complex network where every molecule forms hydrogen bonds with four adjacent molecules. $\pi-\pi$ interactions are supposed to stabilize the structures considerably.

B. From Three- to Two-Dimensional Ordering. To gain information on the 2D ordering of quinacridones, STM measurements have been performed on physisorbed monolayers at the solid/liquid interface. These experiments were also aimed at gaining more insight into the aggregation behavior in solution, as the 2D ordering could give information concerning the possible hydrogen-bonding patterns. Therefore, several substituted quinacridone derivatives were studied and compared to their *N*,*N*′-dimethylated analogues. These experiments were performed on highly oriented pyrolytic graphite (HOPG), which has proven to be an excellent substrate to accommodate alkyl-containing compounds.

Parts A and B of Figure 9 are STM images of monolayers of **2** adsorbed at the liquid/graphite interface. The solvent used is a mixture of 1,2,4-trichlorobenzene (1,2,4-TCB) and 1-octanol. These solvents were selected because of their low vapor pressure, which facilitates the STM experiments in a liquid drop. Only this combination of solvents was successful for imaging purposes. Dissolving the compound in 1,2,4-TCB leads to aggregation, which is manifested by the red color of the solution. Addition of a few drops of 1-octanol turns the solution yellow. In 1-phenyloctane, the compound forms a gel or precipitates. Apparently, it is necessary to destroy the aggregation in solution to at least a certain extent before adsorption takes place or, more precisely, before an "immobilized" 2D layer is formed. Indeed, immobilization of the molecules on the substrate is a prerequisite for obtaining high-resolution images. The molecules are ordered in lamellae or rows on the surface. ΔL_1 (4.3 ± 0.2 nm) defines the center-to-center distance between two adjacent rows of the QNC cores.

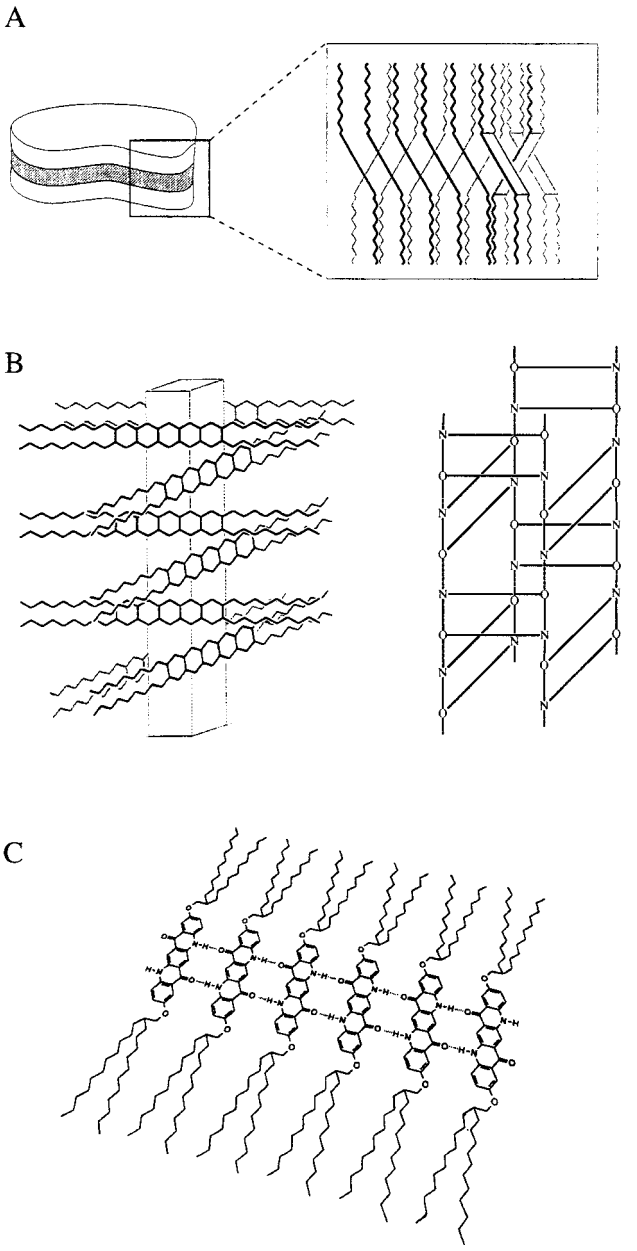

Figure 8. Drawings representing the proposed aggregate structures of **2** (A and B) and **7** (C). (A) A two-dimensional aggregate with molecules interacting on the basis of the hydrogen-bonding pattern shown in Figure 7B. (B) A more tubular kind of aggregate. The hydrogen-bonding pattern is modeled in more detail in the right panel. (C) A linear coplanar ordering of the chromophores in the aggregate.

The brighter bands are attributed to the locations of the chromophores. The long axis of the QNC unit is not oriented perpendicular to the lamella axis but makes an angle between 20° and 25°. Alkyl chains are not resolved and this suggests a rather high mobility and a nonideal packing on the graphite surface. Both images show many defects and streaky features. This is typical for highly dynamic and nonstable monolayers. The center-to-center distance between adjacent QNC units is 0.85 ± 0.1 nm. As modeling shows that the ideal distance between adjacent coplanar QNCs is ≈0.64 nm to allow for optimal hydrogen bonding, the data suggest that hydrogen bonding does not contribute to the 2D ordering. The dots in the middle of two adjacent QNC rows might be attributed to the alkyl chain ends. The

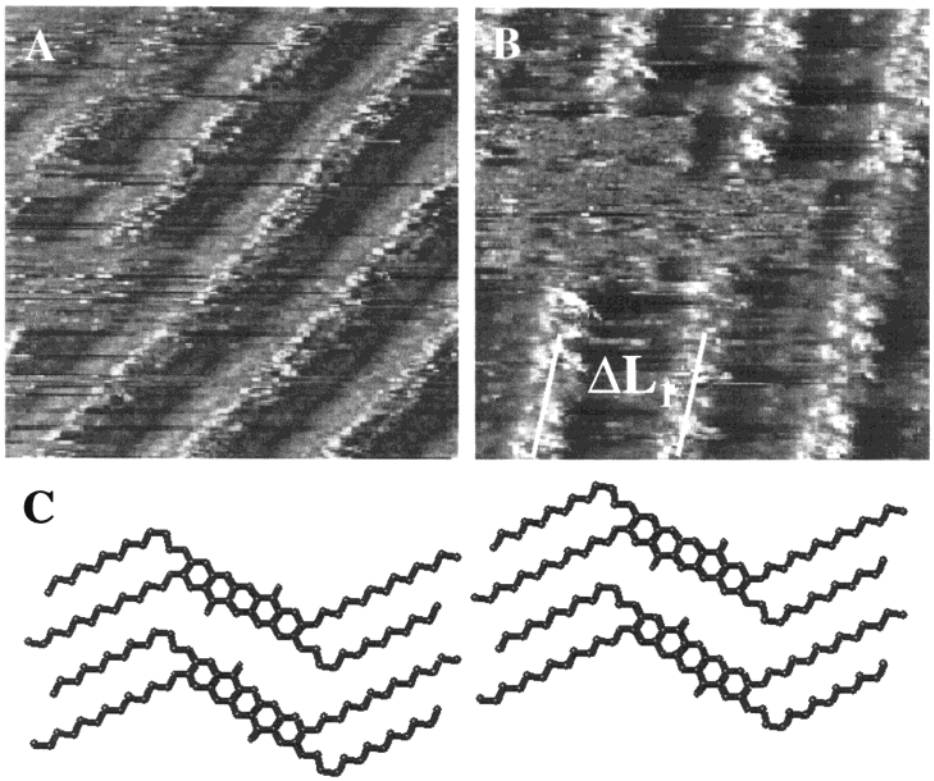

Figure 9. STM images of monolayers of **2** adsorbed at the liquid/graphite interface. The solvent is a mixture of 1,2,4-trichlorobenzene and 1-octanol. (A) Image size: 19 × 19 nm^2. (B) Image size: 13.3 × 13.3 nm^2. ΔL_1 is the lamella width. (C) Model representing a possible 2D ordering on graphite.

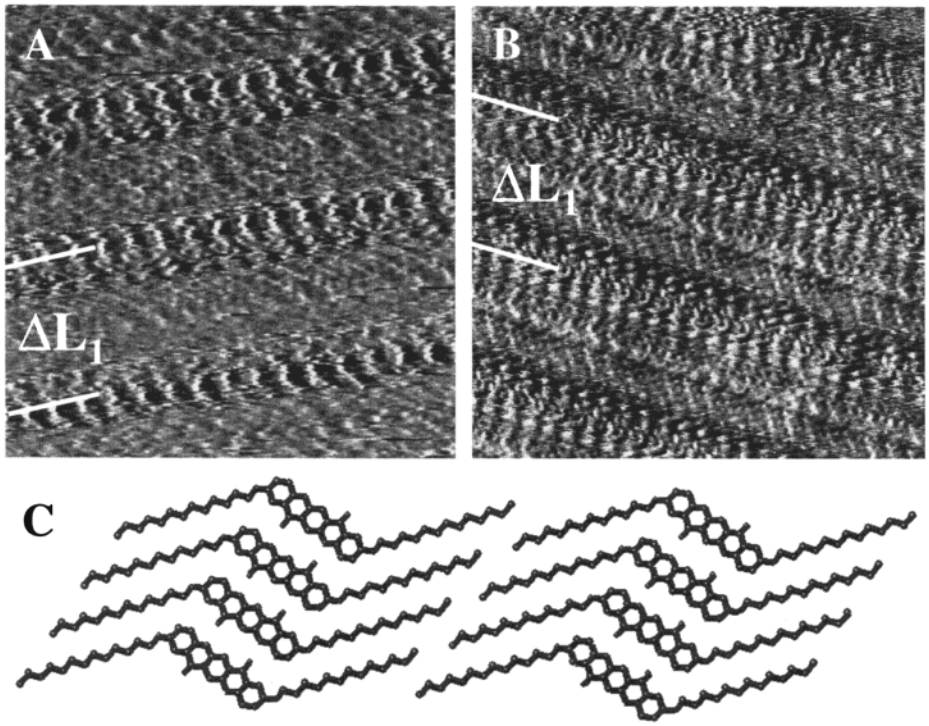

Figure 10. STM images of monolayers of **7** adsorbed at the liquid/graphite interface. The solvent is 1-undecanol. (A) Image size: 10 × 10 nm^2. (B) Image size: 13 × 13 nm^2. ΔL_1 is the lamella width. (C) Model representing a possible 2D ordering on graphite.

orientation of the alkyl chains could not be directly deduced from the images. A tentative model for the 2D ordering of these molecules is given in Figure 9C.

Figure 10A,B represents STM images of a two-dimensional monolayer of **7** physisorbed at the liquid/graphite interface. 1-Octanol and 1-undecanol were used as solvents. Also in these images, the QNC chromophores can be distinguished from the aliphatic chains as they are characterized by a higher tunneling current. The chromophores are again lined up in rows. It appears as if the orientation of the long axis of the chromophores is perpendicular to the lamella axis. In contrast to

monolayers of **2**, the intermolecular distance between QNC chromophores in a row is reduced considerably. The distance is only 0.66 ± 0.02 nm, which suggests that the QNC chromophores form hydrogen bonds. The width of a lamella is 3.9 ± 0.2 nm. The alkyl chains are not interdigitated. The monolayers of **7** show an increased stability with respect to **2** adlayers. This is expressed by the fact that some images show "single" lamellae[44] on an otherwise "empty" graphite surface. This indicates that the intermolecular forces within one lamella are sufficiently high to lower the mobility of the molecules at the surface. It is most likely that hydrogen bonds are the stabilizing forces. Moreover, the existence of single lamellae suggests that the stabilizing intermolecular interactions within a lamella are stronger than those between molecules in adjacent lamellae. Indeed, data analysis shows that the alkyl chains of molecules in adjacent lamellae are not interdigitated and, as such, the interaction between adjacent lamellae will be minimal. The formation of single lamellae under analogous experimental conditions has also been reported for a symmetric bis-urea derivative ($H_{25}C_{12}$−NHCONH−$C_{12}H_{24}$−NHCONH−$C_{12}H_{25}$).[45] This compound contains two urea groups and is able to form strong intermolecular hydrogen bonds (eight in total) with adjacent molecules in the same lamella. Analysis of the data of **7** shows that only one "arm" of the branched alkyl chain is adsorbed on the surface because of steric demands. It has been found more often that an alkyl chain or a part thereof is not in contact with the substrate and is directed to the supernatant solution.[46−49] Figure 10C represents a tentative model for the two-dimensional ordering of these molecules on the graphite surface. Only the adsorbed alkyl part is indicated in the model. Note that this model only represents one of several polymorphous structures.

STM experiments on the *N*,*N*′-dimethyl derivatives (see Supporting Information) show that the intermolecular distance of these derivatives is very close to the value observed for **2**, which supports the idea that **2** is not capable of forming a linear coplanar ordering of the chromophores. In contrast, the data indicate that **7** forms hydrogen bonds when the chromophores adopt a linear coplanar ordering.

Concluding Remarks

These observations are in line with the aggregation model proposed for **2** and **7** in solution in section A based upon the IR experiments. The STM experiments show that **2** cannot adopt a stable ordering when the quinacridone chromophores are lying in the same plane. Because of steric demands of the alkyl chains, hydrogen bonding is prohibited. On the other hand, this compound shows distinct aggregation behavior in solution and it has been proven independently that hydrogen bonding plays a key role in stabilizing the aggregates. The STM experiments show that **7** is capable of forming hydrogen bonds when the QNCs are lying in the same plane. These results, in combination with the IR experiments, strongly support the aggregation models as proposed in section A. STM aided in understanding the intermolecular interactions that are involved in the formation of the aggregates.

Acknowledgment. The authors thank BASF A.G., the Volkswagen Stiftung, DWTC, through IUAP-IV-11, the F.W.O.-Vlaanderen, and ESF SMARTON for financial support. S.D.F. thanks the Fund for Scientific Research−Flanders (FWO) for a postdoctoral fellowship. The collaborations were made possible thanks to the TMR project SISITOMAS.

Supporting Information Available: STM images and discussion on the *N*,*N*′-dimethylated derivatives (**3** and **8**) of the compounds studied along with STM images of compound **5** (PDF). This material is available free of charge via the Internet at http://pubs.acs.org.

CM011053Y

(44) "Single" lamellae do not have lamellae adjacent to them. It is rare to find these structures at room temperature at the liquid/graphite interface. Normally, molecules appear in domains. We find these arrangements only for compounds that combine the following properties: strong intermolecular interactions between adjacent molecules within a lamella; weak intermolecular interactions between adjacent lamellae; strong adsorbate−substrate interactions.

(45) De Feyter, S.; Grim, P. C. M.; van Esch, J.; Kellogg, R. M.; Feringa, B. L.; De Schryver, F. C. *J. Phys. Chem. B* **1998**, *102*, 8981−8987.

(46) Stevens, F.; Dyer, D. J.; Müller, U.; Walba, D. M. *Langmuir* **1996**, *12*, 5625−5629.

(47) Gorman, C. B.; Touzov, I.; Miller, R. *Langmuir* **1998**, *14*, 3052−3061.

(48) De Feyter, S.; Grim, P. C. M.; van Esch, J.; Kellogg, R. M.; Feringa, B. L.; De Schryver, F. C. *J. Phys. Chem. B* **1998**, *102*, 8981−8987.

(49) De Feyter, S.; Gesquière, A.; De Schryver, F. C.; Meiners, C.; Sieffert, M.; Müllen, K. *Langmuir* **2000**, *16*, 9887−9894.